

NUMERICAL SIMULATION OF LAMINAR FLOW OVER SHALLOW CAVITIES

Paulo S. Zidanski – zidanski@aer.ita.cta.br

M. A. Ortega - ortega@aer.ita.cta.br

Nide G. C. R. Fico Jr. – nide@aer.ita.cta.br

Instituto Tecnológico de Aeronáutica, Divisão de Engenharia Aeronáutica,
São José dos Campos, 12228-900, SP, Brasil.

Abstract. *This paper reports on a series of numerical simulations of laminar flows over two-dimensional cavities. Five different aspect ratios, ranging from [1:9.6] to [1:28], were considered. The calculations pointed out that for the aspect ratios studied the flow topology was sensitive to this parameter. The aspect ratio plays a direct influence upon the number and the position of the flow vortices inside the laminar cavity. The numerical results were very sensitive to the inlet velocity profile, which is closely related to be boundary layer thickness upstream of the cavity. The SIMPLER numerical algorithm developed by Patankar was used to solve the discrete equations on a staggered grid. The interpolation functions are based upon the power law scheme.*

Key-Words: *viscous flow, incompressible flow, cavity, numerical method*

1 INTRODUCTION

The flow over cavities is of great interest as it is related to various engineering applications. Aung (1983) found, experimentally, that for laminar forced convection, the local heat transfer distribution on the cavity floor has a maximum value located between the midpoint of the cavity floor and the downstream wall. Bhath and Aung (1984) numerically simulated the 2-D, laminar flow over cavities and showed that the heat transfer inside a cavity is a function of its aspect ratio. Pereira and Sousa (1995) studied both numerically and experimentally the unsteady flow inside cavities. The present authors' interest in such flows is due to their research related to the flow over solar energy collectors. As it is well known in the literature, such devices loose energy to the ambient around it mainly by forced convection due to the wind blowing over its upper surface. The film coefficient is directly related to the wind velocity impinging over the solar collector. The use a wind barrier around the collector perimeter will create a re-circulation region on it's surface, as seen in Fig. 1, diminishing the wind velocity and, consequently the heat transfer film coefficient and the heat loss.

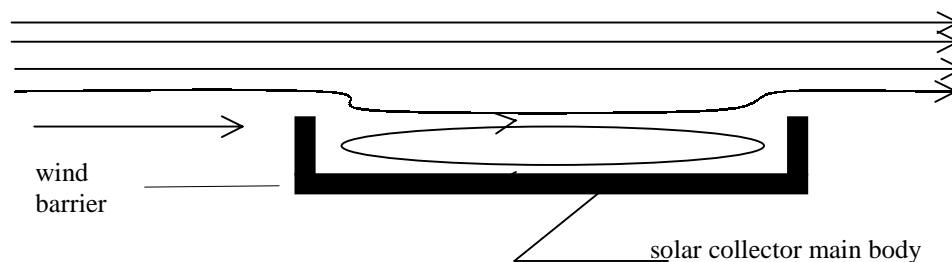


Figure 1: – Sketch of the flow over a solar collector with wind barrier.

The resemblance of such flow to the ones over cavities motivated this work. In order to prepare for the evaluation of the heat transfer from the bottom of the cavity, which represents the collector main body, the isolated fluid mechanics problem will be solved first. The present effort is, therefore, related to numerical analysis of laminar flows over cavities. This is the first stage towards the final simulation of the turbulent heat transfer problem. Up to this point the following influences upon the topology and flow along the cavity were investigated by the authors: (i) Type of velocity profile of the flow approaching the cavity; (ii) Inlet Reynolds number, based on the cavity depth; (iii) Cavity aspect ratio. One might argue that the presence of the wind barrier might impact the oncoming flow by creating a re-circulation zone that does not appear in flows over shallow cavities. Nevertheless, a good understanding of flows over cavities is an important phase of the present research effort.

Sinha et al (1982) made an experimental study of the flow over cavities of various aspect ratios. In their work these authors classified the cavity as open or closed based upon the number of re-circulating bubbles and the position that they occupy inside the cavity. Their results are used in the present work as one of the code validation tests. Prior to use the code for the simulation of the laminar flow over cavities other validation cases were computed, namely: the laminar flows over a flat plate and over a backward-facing step.

2. THEORETICAL FORMULATION AND NUMERICAL METHOD

The mathematical model here considered are the two-dimensional, incompressible, Navier-Stokes equations written for a Cartesian coordinate frame. The partial differential equations are solved numerically by a finite volume algorithm, called SIMPLER (Patankar, 1980), on a staggered Cartesian mesh. The convective and diffusive fluxes are calculated at the volumes' interfaces with the power-law interpolation scheme. The SIMPLER algorithm is a semi-implicit method. The iteration procedure starts with an arbitrary velocity field from which results a pressure distribution. After the pressure field is calculated a new velocity distribution is obtained from the momentum equations. The improved velocity field is used to solve the pressure equation. The process is repeated until convergence is obtained.

2.1 Boundary Conditions. At the solid walls the non-slip boundary conditions are enforced, that is, $u = v = \text{zero}$. At the upper boundary as well as at the exit section a parabolic type of boundary condition is used. This is equivalent to saying that the property gradients at these boundaries are zero. A parabolic boundary condition is interesting in the sense that it is non-reflexive. In other words, no spurious perturbation is reflected back into the computational domain. Finally, at the entrance plane two different velocity profiles were experimented, namely: a uniform one and a Blasius laminar boundary layer profile. As expected, the choice of the velocity distribution at the inlet plane has a direct influence on the boundary layer thickness at the separation point and, consequently, on the flow properties inside the cavity. Figure 2 displays the problem geometry.

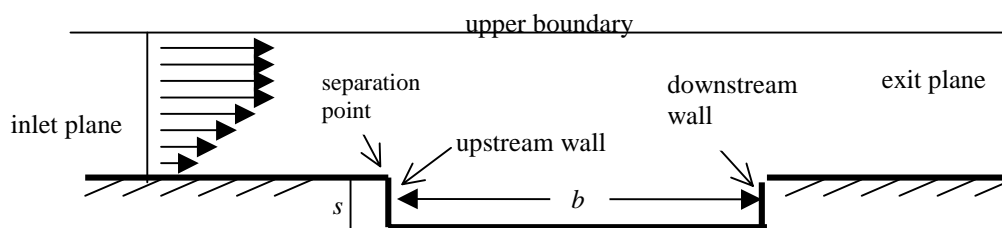


Figure 2: Problem geometry and nomenclature.

3. CODE VALIDATION

To validate the numerical code classical test cases were solved. The well-known Blasius profile was reproduced for the flat plate. The velocity u is nondimensionalized by the undisturbed velocity u_∞ . The dimensionless coordinate normal to the wall is the Blasius variable, η (see Fig. 3).

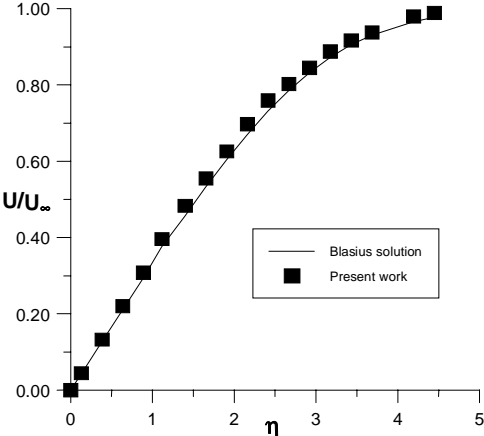


Figure 3: Comparison of the numerical solution for laminar flow and the exact profile.

Another very interesting geometry to validate numerical codes is the backward-facing step. The reattachment length calculated compared well with the experimental and computational values reported by Fletcher (1988) as can be observed in Fig. 4.

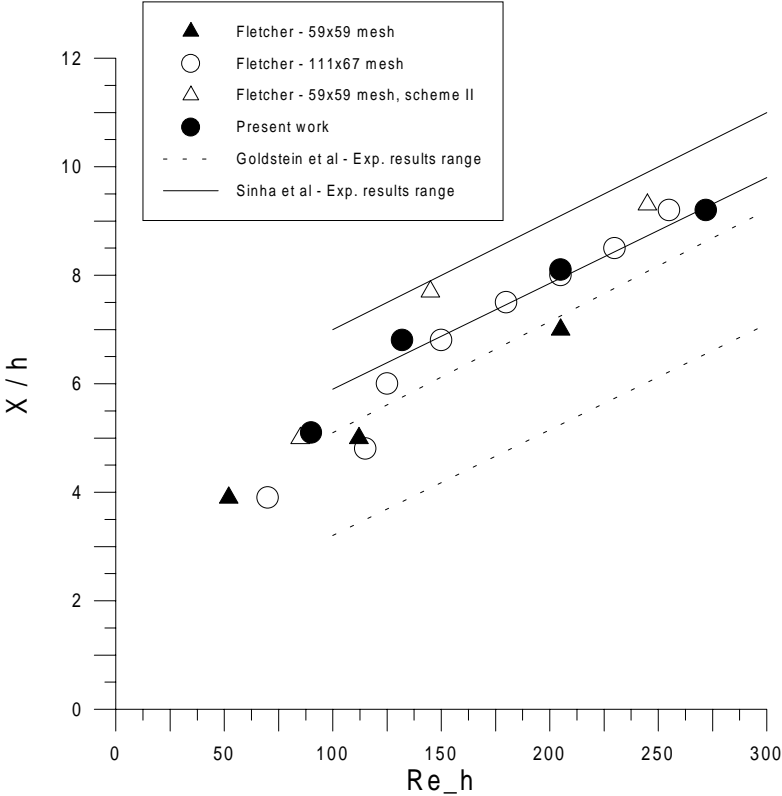


Figure 4: Non-dimensional reattachment length, x/h , as function of the Reynolds number based on the step height, h .

4. COMPUTATIONAL GRID

A typical computational grid is shown in Fig. 5. The inlet boundary is located at four cavity depths, $4s$, upstream of the separation point. The outlet boundary is at a distance of $6.8s$ from the downstream wall. In spite of the parabolic character of the upper boundary, numerical experiments showed that a minimum of $10s$ was necessary in order to avoid spurious interference on the numerical solution. The grid was refined close to the wall and to the cavity entrance and exit planes. Figure 5(b) shows a close-up of the grid at the separation point. The computational domain is sub-divided by an orthogonal, non-uniform mesh. Grid points are clustered near the walls and at regions where the strongest gradients are expected. The stretching factor used in both directions is never greater than 1.10 in order to minimize numerical errors. The exception was the longer cavity because otherwise a prohibitive number of points would be necessary.

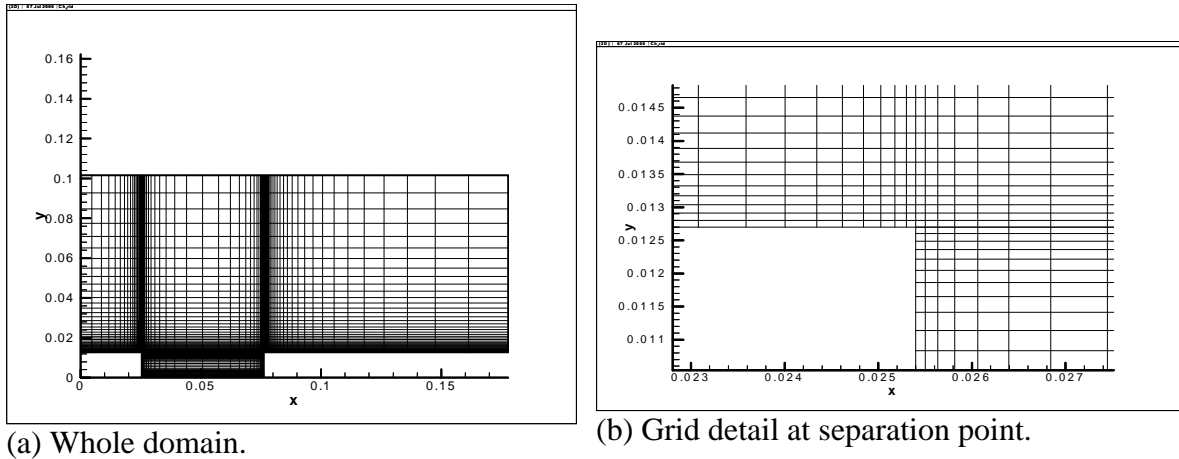


Figure 5: Typical computational grid.

5. RESULTS

The results obtained focus on three important aspects of the simulation of flows over cavities. These are the influence of the incoming velocity profile, of the cavity aspect ratio and of the Reynolds number upon the flow topology and the flow overall characteristics.

Influence of the inlet velocity profile. In order to assess the influence of the inlet velocity profile upon the flow, the following geometry and physical characteristics were considered: (i) Aspect ratio [1:28]; being the cavity depth equal to 0.625 cm ; (ii) Inlet free-stream velocity, $U_\infty = 1.8\text{ m/s}$; (iii) Reynolds number based upon the cavity depth, $Re_s = 662$. These values were considered because there was experimental data available (Sinha et al, 1982).

Many numerical experiments were done; the most representatives are shown in Fig. 6. The reader can observe the plot of the pressure coefficient, c_p , along the cavity floor for three different cases: (a) Uniform profile at the entrance section located at a distance of four cavity depths, $4s$, upstream of the separation point; (b) A Blasius profile, at the same entrance plane, such that the boundary layer thickness, δ , is equal to 0.54 cm at the upstream wall station; (c)

A Blasius profile, at the same distance $4s$ upstream of the first corner, such that $\delta = 1.4 \text{ cm}$ at the upstream wall station. Case (c) is the one that gave the best c_p distribution when compared with the experimental data. This is confirmed by Fig. 7, where the numerical and experimental pressure distributions are compared for the same geometry and flow conditions mentioned above [case (c)]. Therefore all cases that are reported hereafter, independently of the specific conditions, tries to mimic case (c) above.

The important point here is related to the boundary layer thickness at the upstream corner of the cavity – the main separation point. Case (c) above reproduces the experimental value of $\delta = 1.4 \text{ cm}$ at this station with great accuracy. On the other hand, case (a) and (b) give values of δ that deviate considerably from the experimental one. For this reason these cases are unable to reproduce the experimental c_p distribution.

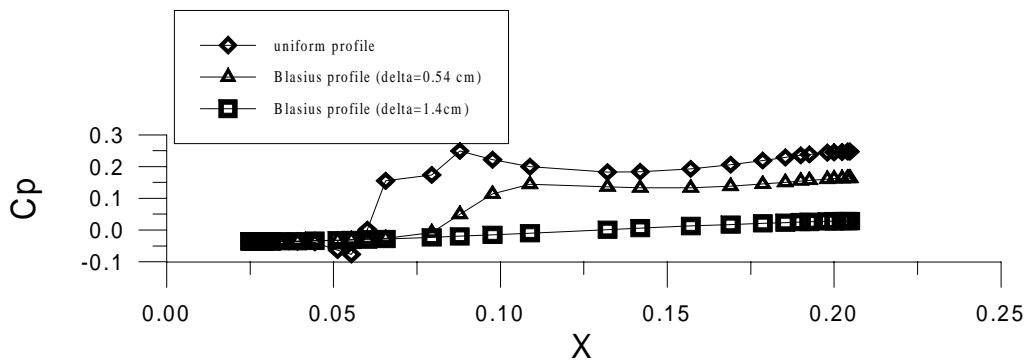


Figure 6: Influence of the inlet velocity profile upon the c_p distribution at the cavity floor.

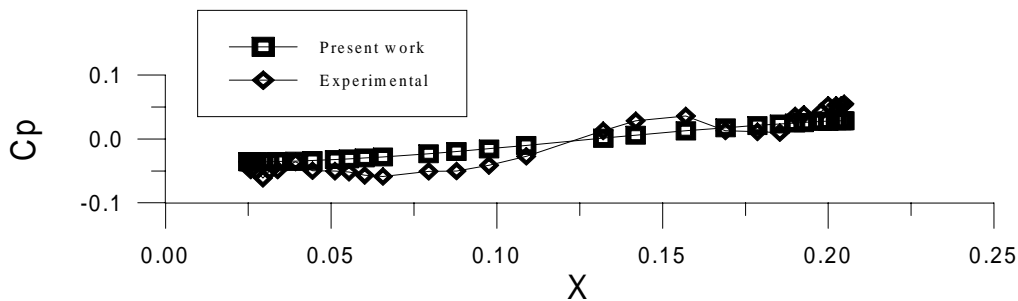


Figure 7: Comparison of the c_p distribution at the cavity floor with experimental data.

Influence of the Reynolds number. For this investigation, a cavity having a 1:12 aspect ratio was considered. The Reynolds number based upon the cavity depth, Re_s , was varied from 147 to 662. For all cases, two bubbles were found, as expected, but the Reynolds number influenced not only the location of the bubbles but also their shape. The first simulation was done for $Re_s = 147$ which correspond to a free stream velocity $u_{in} = 0.4 \text{ m/s}$. In this case it was observed that the flow penetrates the cavity touching its bottom. The first bubble has its center at $(x/s) = 2.4$ while the second and smaller one is centered at $(x/s) = 11.6$. As the Reynolds number increased, by making U_∞ larger, the bubbles centers moved closer to each other. For $U_\infty = 1.8 \text{ m/s}$ ($Re_s = 662$) the center of the bigger re-circulating bubble was found to be at $(x/s) = 8.9$, while the smaller bubble barely moved, having its center now located at $(x/s) = 11.2$. This was the closest the two centers came to each other. Except for the

lower Reynolds number, the flow field did not have a stagnation point at the cavity floor. This is explained by the greater inertia of the incoming flow as the Reynolds number increases. Thus for $Re_s=294, 441, 662$ the two re-circulation zones simply relocate inside the cavity. In Fig. 8 it is sketched, not to scale, the flow topology for cases $Re_s = 147$ and 662 discussed above. A drawing of the flow topology was made, because the aspect ratios used in the calculations made it impossible to show the streamlines resulting from the numerical simulation without distorting them.

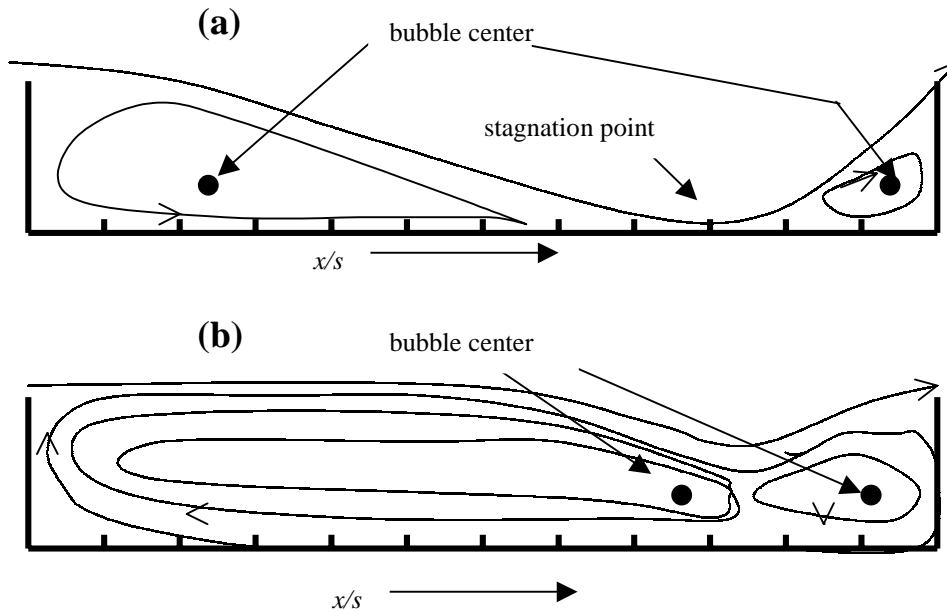


Figure 8: Sketch of the flow over a 1:12 cavity for: (a) $Re_s = 147$ and (b) $Re_s = 662$.

Figure 9 shows a zoomed view of the streamlines, obtained from the numerical solution, close to the cavity downstream wall ($Re_s=662$). It is apparent that the bubble is “flattened”, that is, the streamlines are elongated. The evolution of the flow topology as Re_s increases indicates towards a merging of the two bubbles. However, it was not possible to confirm this tendency in the limit, because the code diverged consistently. The point here is that the Reynolds number based on the cavity length reached values corresponding to turbulent flow near the downstream wall.

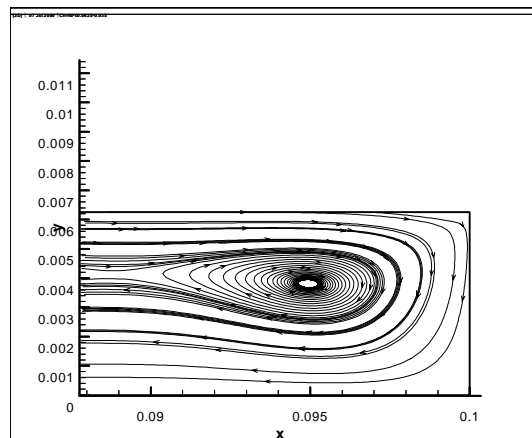


Figure 9: Streamlines for the smaller bubble for $Re_s = 662$ [1:12].

Influence of the cavity aspect ratio. Finally the influence of the aspect ratio upon the pressure coefficient along the cavity floor was investigated. The Reynolds number based on the cavity depth, Re_s , was kept constant and equal to 662. The aspect ratios used for the simulations were [1:9.6], [1:10], [1:12], [1:18] and [1:28]. The sketches of the flow topology for some of these cases are shown in Fig. 10. The flow is very different for each of the three aspect ratios. The shortest cavity presented a flow pattern in which only one re-circulating bubble appeared. It is important to emphasize that the numerical code is being very accurate in reproducing the flow topology. This is confirmed by the two-bubble formation for the slightly greater aspect ratio [1:10], as reported in the literature (Sinha et al., 1982). The much longer cavity tends to behave like a sequence of a backward facing step, a flat plate and a forward facing step. Thus the flow separates abruptly at the upstream wall, reattaches somewhere on the cavity floor and close to the downstream wall another separated region is formed.

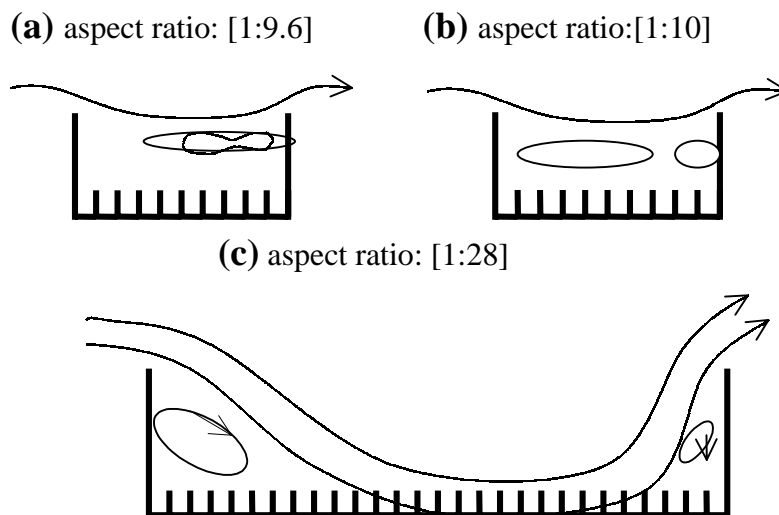


Figure 10: Sketch of the flow for several aspect ratios and $Re_s = 662$.

The pressure coefficient distributions associated with four different aspect ratios are shown in Fig. 11. Notice that there is a well-defined valley for the smaller aspect ratio, which corresponds to the center of the only re-circulation bubble formed [Fig. 11(a)]. The higher aspect ratios presented a c_p distribution very similar to the one shown in Fig. 7. For these cases, a much smoother distribution of the pressure coefficient along the cavity floor is found indicating “weaker” vortices associated to the longer cavities.

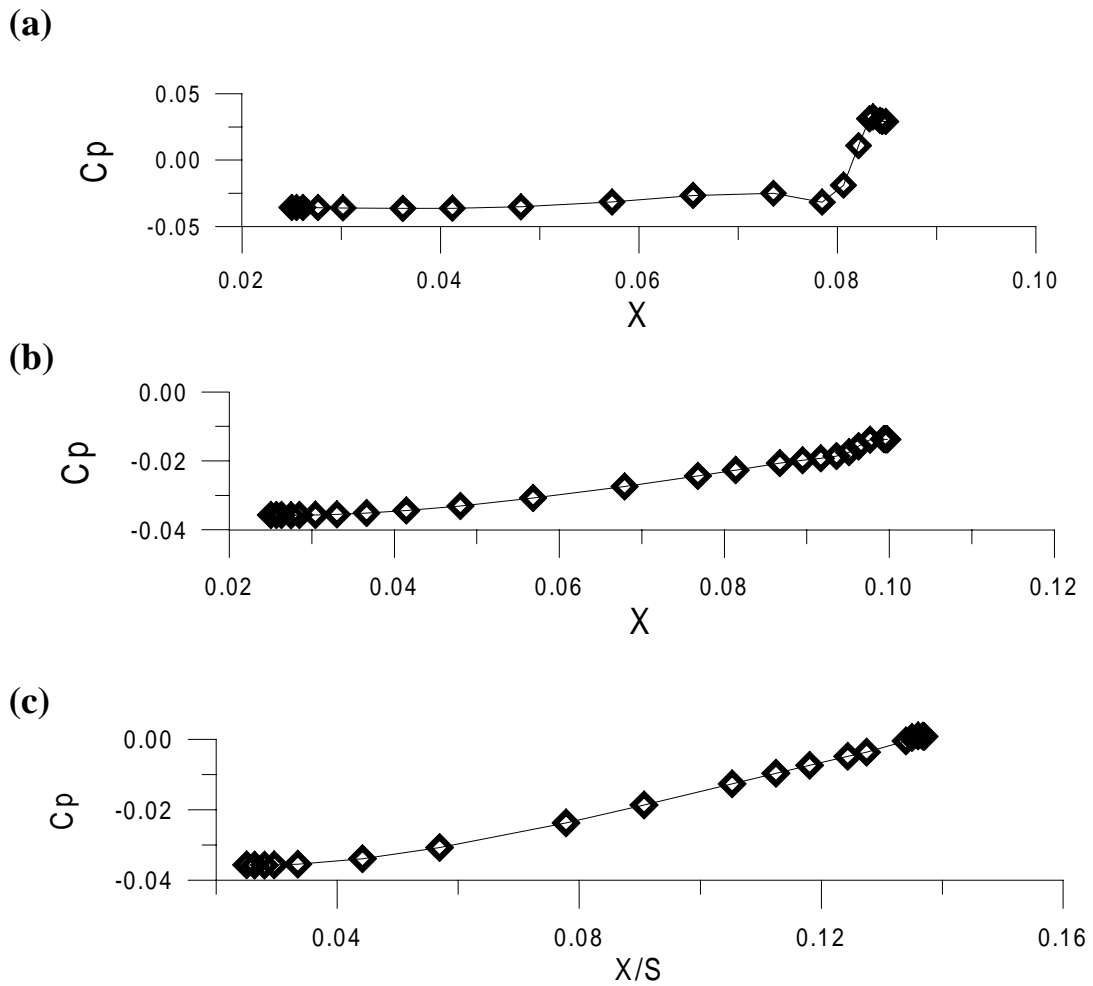


Figure 11: c_p distribution at the cavity floor for: (a) 1:9.6, (b) 1:12, (c) 1:18.

6. CONCLUSION

The laminar flow inside cavities of aspect ratios ranging from [9.6] to [28] was simulated. The flow topology obtained is in agreement with experimental data. It became apparent that the inlet velocity profile has a direct influence upon the flow inside the cavity. The aspect ratio is determinant as to the number and the shape of re-circulating zone will exist. This is certainly an essential factor in the design of low loss solar energy collectors. Further numerical simulations are certainly needed. The authors will concentrate next on aspect ratios ranging from 5 to 10 as these values are currently used for solar energy collectors. Another important aspect to investigate is the influence of the wind barrier upon the oncoming flow.

Acknowledgements

The work of M. A. Ortega was supported in part by the Brazilian agency, National Council of Scientific and Technological Development – CNPq, under grant 522413/96-0.

REFERENCES

- Aung, W., 1983, “An experimental Study of Laminar Heat Transfer Downstream of Backsteps,” ASME Journal of Heat Transfer, Vol. 105, pp. 823-828.

- Bhath A. and Aung W., 1984, "Finite Difference Analysis of Laminar Separated Forced Convection in Cavities," ASME Journal of Heat Transfer, Vol. 106, pp. 49-54.
- Fletcher, C.A.J., 1988, Computational Techniques for Fluid Dynamics, Vol. II, Springer Series in Computational Physics, Springer Verlag, Berlin.
- Sinha, S.N., Gupta A.K., and Oberai, M.M., 1982, "Laminar Separating Flow Over Backsteps and Cavities. Part II: Cavities," AIAA Journal, Vol. 20, n. 3, pp. 370-375.
- Patankar, S.V., 1980, Numerical Heat Transfer and Fluid Flow, Hemisphere, Washington, D.C.
- Pereira, J.C.F. and Sousa, J.M.M, 1995, "Experimental and Numerical Investigation of the Flow Oscillations in a Rectangular Cavity," ASME Journal of Fluids Engineering, Vol. 117, pp. 68-74.